[CANCER RESEARCH 64, 4931–4941, July 15, 2004]

AEE788: A Dual Family Epidermal Growth Factor Receptor/ErbB2 and Vascular Endothelial Growth Factor Receptor Tyrosine Kinase Inhibitor with Antitumor and Antiangiogenic Activity

Peter Traxler,[1] Peter R. Allegrini,[1] Ralf Brandt,[2] Josef Brueggen,[1] Robert Cozens,[1] Doriano Fabbro,[1] Konstantina Grosios,[1] Heidi A. Lane,[1] Paul McSheehy,[1] Jürgen Mestan,[1] Thomas Meyer,[1] Careen Tang,[3] Markus Wartmann,[1] Jeanette Wood,[1] and Giorgio Caravatti[1]

[1]Novartis Institutes for Biomedical Research, Oncology Research, Basel, Switzerland; [2]Vivo Pharm Pty, Ltd., Thebarton, Australia; and [3]Lombardi Cancer Center, Georgetown University Medical Center, Washington, DC

ABSTRACT

Aberrant epidermal growth factor receptor (EGFR) and ErbB2 expression are associated with advanced disease and poor patient prognosis in many tumor types (breast, lung, ovarian, prostate, glioma, gastric, and squamous carcinoma of head and neck). In addition, a constitutively active EGFR type III deletion mutant has been identified in non-small cell lung cancer, glioblastomas, and breast tumors. Hence, members of the EGFR family are viewed as promising therapeutic targets in the fight against cancer. In a similar vein, vascular endothelial growth factor (VEGF) receptor kinases are also promising targets in terms of an antiangiogenic treatment strategy. AEE788, obtained by optimization of the 7*H*-pyrrolo[2,3-*d*]pyrimidine lead scaffold, is a potent combined inhibitor of both epidermal growth factor (EGF) and VEGF receptor tyrosine kinase family members on the isolated enzyme level and in cellular systems. At the enzyme level, AEE788 inhibited EGFR and VEGF receptor tyrosine kinases in the nM range (IC_{50}s: EGFR 2 nM, ErbB2 6 nM, KDR 77 nM, and Flt-1 59 nM). In cells, growth factor-induced EGFR and ErbB2 phosphorylation was also efficiently inhibited (IC_{50}s: 11 and 220 nM, respectively). AEE788 demonstrated antiproliferative activity against a range of EGFR and ErbB2-overexpressing cell lines (including EGFRvIII-dependent lines) and inhibited the proliferation of epidermal growth factor- and VEGF-stimulated human umbilical vein endothelial cells. These properties, combined with a favorable pharmacokinetic profile, were associated with a potent antitumor activity in a number of animal models of cancer, including tumors that overexpress EGFR and or ErbB2. Oral administration of AEE788 to tumor-bearing mice resulted in high and persistent compound levels in tumor tissue. Moreover, AEE788 efficiently inhibited growth factor-induced EGFR and ErbB2 phosphorylation in tumors for >72 h, a phenomenon correlating with the antitumor efficacy of intermittent treatment schedules. Strikingly, AEE788 also inhibited VEGF-induced angiogenesis in a murine implant model. Antiangiogenic activity was also apparent by measurement of tumor vascular permeability and interstitial leakage space using dynamic contrast enhanced magnetic resonance imaging methodology. Taken together, these data indicate that AEE788 has potential as an anticancer agent targeting deregulated tumor cell proliferation as well as angiogenic parameters. Consequently, AEE788 is currently in Phase I clinical trials in oncology.

INTRODUCTION

The epidermal growth factor receptor (EGFR) and vascular endothelial growth factor (VEGF) receptor (VEGFR) tyrosine kinase families belong to the best-studied and most attractive receptor tyrosine kinase targets for cancer chemotherapy; their role in signal transduction and the development of cancer is well described (for recent reviews on EGFR and VEGFR refer to Refs. 1–8).

Much evidence has accumulated that the EGFR and its family members are strongly implicated in the development and progression of numerous human tumors, including breast, lung, colorectal, ovarian, glioma, prostate, bladder, and head and neck. Indeed, overexpression of EGFR/ErbB2 and ErbB ligands is correlated with advanced disease and poor patient prognosis (9). In addition, truncated EGFRs have also been detected, the most common of which is the EGFRvIII mutant (10, 11). This gene is often amplified in tumor cells (*e.g.*, glioma, breast, and lung). Moreover, a subset of invasive breast carcinoma expresses EGFRvIII, whereas no detectable levels of EGFRvIII occur in normal breast tissue. The type III truncated EGFR lacks elements of the extracellular domain and is consequently unable to bind a ligand. Despite this, it displays constitutive kinase activity (3). These unique features make the mutant-EGFRvIII a potential target for antitumor intervention.

Angiogenesis is the process by which new blood vessels extend from established blood vessels (12–14). Solid tumors, regardless of their type and origin, cannot grow beyond a certain size (1–2 mm^3) until they establish a blood supply by inducing the formation of new vessels sprouting from existing host capillaries (15–17). VEGF, a mitogen specific for vascular endothelial cells, is considered to play a key role in the angiogenic process and is secreted by tumor cells and macrophages (18). The angiogenic signal is transmitted via cell surface receptors (*KDR* and *Flt-1*) located on the host vascular endothelium, which have intracellular tyrosine kinase activity (for recent reviews refer to Refs. 19 and 20). Inhibition of VEGF-induced angiogenic signals will selectively target the tumor-associated vessels, because cell division of endothelial cells in the normal vasculature is a very rare event. VEGF (also known as vascular permeability factor) is also a potent inducer of vascular permeability (20). A selective VEGFR kinase inhibitor will influence tumor growth by inhibiting tumor vascularization and should not directly inhibit tumor cell growth. It is expected that such a compound will be most effective in a minimal disease situation, before tumors establish an extensive vasculature. Antiangiogenic therapy through inhibition of VEGF-mediated effects is expected to be safer and better tolerated in cancer patients as compared with therapy with standard cytotoxic agents.

The attractiveness and "drugability" of the ErbB and VEGFR families have led to several antibodies (6, 21–23) and small molecules with promising *in vitro* and *in vivo* preclinical profiles being advanced into clinical trials (5). Several of them have already provided a clinical proof of concept. Currently, there are at least four low molecular weight, ATP-competitive EGFR tyrosine kinase inhibitors and six VEGFR tyrosine kinase inhibitors (2, 7, 8, 24–26) in different stages of clinical development (Refs. 5, 27–29 for recent reviews). The EGFR inhibitor Iressa (30) has been launched in Japan and recently in the United States for use in refractory non-small cell lung cancer. The most advanced VEGFR tyrosine kinase inhibitors are PTK787/ZK222584 (codeveloped by Novartis/Schering AG, Berlin, Germany; Refs. 31–34) and ZD6474 (35–37). PTK787/ZK22584 entered Phase III combination studies recently in patients with colorectal cancer.

Received 11/25/03; revised 5/5/04; accepted 5/19/04.

The costs of publication of this article were defrayed in part by the payment of page charges. This article must therefore be hereby marked *advertisement* in accordance with 18 U.S.C. Section 1734 solely to indicate this fact.

Requests for reprints: Peter Traxler, Novartis Institutes for Biomedical Research, Oncology Research, Klybeckstrasse, CH-4002 Basel, Switzerland; Phone: 41-61-696-5286; Fax: 41-61-696-3429; E-mail: peter.traxler@pharma.novartis.com.

It has been shown that expression of proangiogenic molecules (such as VEGF) by tumor cells can be stimulated by epidermal growth factor/ErbB2 receptor signaling (38, 39, 41). Indeed, antiangiogenic effects have been described for several ErbB family inhibitors. Specifically, antiangiogenic properties (*e.g.*, reduction of the diameter and volume of tumor blood vessels and reduction of vascular permeability) have been attributed to the ErbB2 antibody Herceptin, using an experimental mouse model of human breast cancer that overexpresses ErbB2 (40). Furthermore, decreased tumor cell production of proangiogenic molecules and inhibition of tumor-associated angiogenesis has been demonstrated for small molecule EGFR inhibitors such as Iressa (30) and PKI166 (5, 41, 42). Hence, although it is expected that ErbB receptor inhibitors will have an element of antiangiogenic activity, as well as direct effects on tumor cell proliferation, as part of their activity in human cancer, it was reasoned that additional inhibition of VEGFR activity would act to accentuate the antitumor effects of EGFR/ErbB2 inhibitors. Indeed, in this respect, a recent publication reported encouraging combination effects using an anti-EGFR and an anti-VEGFR-2 (KDR) antibody in a murine model of human colon cancer, including decreased tumor vascularity and increased tumor and endothelial cell apoptosis with the combination (43). Furthermore, recent studies evaluating PKI166 in combination with PTK787/ZK222584 (31) against experimental human non-small cell lung tumors and *NeuT*-driven genetically engineered mouse mammary tumors have demonstrated enhanced (synergistic) antitumor effects in both tumor types (44). These data indicate that, although EGFR/ErbB2 inhibitors can inhibit production of VEGF by tumor cells, a more potent antitumor response is achieved through the concomitant inhibition of both the EGFR/ErbB-2 and VEGF receptors (KDR and Flt-1). The development of inhibitory compounds with combined ErbB/VEGF receptor activities in the same molecule is, therefore, an opportunity to improve antitumor efficacy and to broaden application possibilities.

MATERIALS AND METHODS

Compounds. AEE788, PKI166, and PTK787/ZK222584 (Fig. 1) were synthesized in the Department of Oncology Research at Novartis Institutes for Biomedical Research.

A stock solution of AEE788 for enzyme or cellular assays was prepared in DMSO and then diluted in the optimal medium. The final concentration of DMSO in the incubation mixture did not exceed 0.1% v/v.

The formulation used throughout all of the *in vivo* experiments consisted of solutions or suspension of the compound (AEE788, PKI166, and PTK787/ZK222584) in *N*-methylpyrrolidone and PEG300 1:9 (v/v). The concentration of the compounds was adjusted to allow administration of $\leq$200 μl of total excipient. Solutions/suspensions were prepared just before administration to mice.

Cells and Cell Culture Conditions. Human umbilical vein endothelial cells were obtained from Promo Cell (BioConcept AG, Allschwil, Switzerland) and cultivated *in vitro* according to the recommendations of the supplier. BT-474 human breast carcinoma cells, BALB/3T3 mouse fibroblasts, and A431 human epidermoid carcinoma cells were cultured in DMEM high glucose, 10% FCS, 1% penicillin/streptomycin, and 2 mM glutamine. Chinese hamster ovary cells ectopically expressing human VEGF-receptor KDR were generated by Novartis Institutes for Biomedical Research and cultured in MEM α-medium in presence of 10% FCS, 1% penicillin/streptomycin, and 0.5 mg/ml geniticin G418. HC11 mouse mammary epithelia cells were grown as described previously (45). NCI-H596 human adenosquamous lung cancer cells and DU145 human prostate cancer cells were cultured in RPMI 1640, 10% FCS, and 1% penicillin/streptomycin. SK-BR-3 mammary carcinoma cells were kindly provided by Dr. Nancy Hynes (Friedrich Miescher Institute, Basel, Switzerland) and cultured in Dulbecco's Modified Eagle Medium (DMEM), 10% FCS, and 1% penicillin/streptomycin. BALB/c mouse epidermal keratinocyte cells were kindly provided by Dr. Steward Aaronson (National Cancer Institute, Bethesda, MD) and cultured with DMEM/Ham's F12 medium without calcium, complemented with 5 ng/ml EGF and 5% FCS. T24 transitional bladder carcinoma cells were incubated with MEM-Earls Basic Salt (EBS) medium complemented with nonessential amino acids (1%) and 5% FCS. For *in vivo* experiments, cells were initially cultured in the supplemented medium suggested by the supplier and then used to establish s.c. tumors in BALB/c *nu/nu* mice (from Iffa Credo, Lyon, France). 32D cells transfected with EGFRvIII receptor (EGFRvIII; Ref. 11) were grown in RPMI 1640 (Biofluids, Camarillo, CA), 10% fetal bovine serum (Quality Biological, Inc., Gaithersburg, MD), and 5% WEHI medium. MCF-7- and MCF-7-transfected EGFRvIII cells were grown in Improved Minimum Essential Medium (IMEM) (Biofluids), 10% fetal bovine serum (Quality Biological, Inc.), and 2 mM glutamine. Unless mentioned otherwise, cells were obtained from the American Type Culture Collection (Rockville, MD). All of the cell culture reagents and supplements (FCS, penicillin, and streptomycin) were obtained from Life Technologies, Inc. EGF was obtained from Biomedical Technologies Inc. (Stoughton, MA).

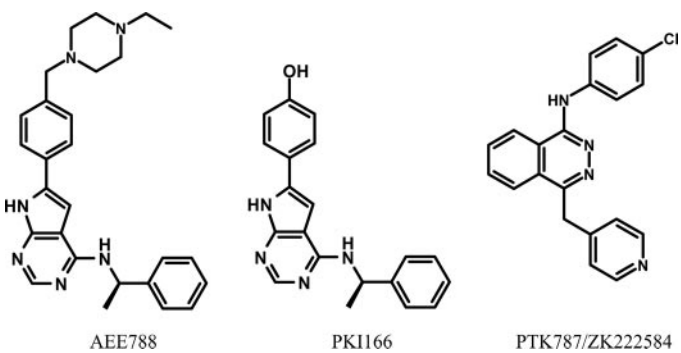

Fig. 1. Structures of AEE788, PKI166, and PTK787/ZK222584.

Ligands and Antibodies. Purified human VEGF was obtained from Dr. Martiny-Baron (Novartis Institutes for Biomedical Research). Recombinant human platelet-derived growth factor (PDGF)-BB for stimulation of the PDGF receptor was obtained from BACHEM AG, Switzerland (product number 4031083.0025). The capture antibody for the KDR-ELISA (Mab 1495.12.14) was originally generated by Harry Towbin (Novartis Institutes for Biomedical Research) and purified from cell culture supernatants with standard methods (protein A-Sepharose). Anti-EGFR monoclonal antibodies used for immunoprecipitation were from Transduction Laboratories (# E12020). Rabbit or goat polyclonal anti-EGFR antibodies used for Western blotting or as second antibody for the EGFR ELISA, respectively, were from Santa Cruz Biotechnology, Inc. (# SC03 or SCO3G). The capture antibody used in the EGFR ELISAs was the anti-EGFR Ab5 from NeoMarkers (MS316-P1ABX). Monoclonal anti-erbB-2 antibodies used for immunoprecipitation were from NeoMarkers, (# MS-32-P1). Rabbit polyclonal anti-erbB-2 antibodies used for Western blotting were from ZYMED (# 28–004). The capture antibody used in the c-erbB2 ELISA was the anti-c-erbB-2 Ab2 from NeoMarkers (# MS229-PABX). Horseradish peroxidase-labeled secondary antirabbit IgG-antibodies used for Western blotting were from Amersham (# NIF824). The enhanced chemiluminescence detection kit used was from Amersham (# 2108). The antiphosphotyrosine-specific monoclonal antibody 4G10 was produced and purified from hybridoma supernatants by standard methods (protein A-Sepharose affinity chromatography). The secondary alkaline phosphatase (AP)-labeled antiphosphotyrosine antibody PY20(AP) was obtained from ZYMED (# 03–7722). AP-labeled antibodies to goat IgG from Sigma (# A8062) were used as tertiary antibodies for the EGFR-ELISA. The substrate to measure AP activity in the capture ELISAs was obtained from Tropix (CDPStar RTU with Emerald II; Cat. No: MS100RY). The Bio-Rad DC Protein Assay kit (Bio-Rad; 500-0111) was used for determination of the protein concentrations of the cell-lysates.

The composition of the lysis buffer for preparation of cell lysates was 50 mM Tris-HCl (pH 7.4), 150 mM NaCl, 5 mM EDTA, 1 mM EGTA, 1.5 mM $MgCl_2$, 1% NP40, 10% glycerol, 2 mM sodium ortho-vanadate, 1 mM phenylmethylsulfonyl fluoride, 80 μg/ml aprotinin, and 50 μg/ml leupeptin.

Protein Kinase Assays. The *in vitro* kinase assays were performed in 96-well plates (30 μl) at ambient temperature for 15–45 min using the recombinant glutathione *S*-transferase-fused kinase domains (4–100 ng, de-

pending on specific activity) prepared as described previously (31, 46). [γ^{33}P]ATP was used as phosphate donor and polyGluTyr-(4:1) peptide as acceptor. With the exception of protein kinase C-α, cyclin-dependent kinase 1/cycB and protein kinase A were protamine sulfate (200 μg/ml), histone H1 (100 μg/ml), and the heptapeptide Leu-Arg-Arg-Ala-Ser-Leu-Gly (known as Kemptide Bachem; Bubendorf, Switzerland), respectively and were used as peptide substrates. Assays were optimized for each kinase using the following ATP concentrations: 1.0 μM (c-Kit, c-Met, c-Fms, c-Raf-1, and RET), 2.0 μM (EGFR, ErbB2, ErbB3, and ErbB4), 5.0 μM (c-Abl), 8.0 μM (Flt-1, Flt-3, Flt-4, Flk, KDR, FGFR-1, and Tek), 10.0 μM (PDGF receptor-β, protein kinase C-α, and cyclin-dependent kinase 1), and 20.0 μM (c-Src and protein kinase A). The reaction was terminated by the addition of 20 μl 125 mM EDTA. Thirty μl (c-Abl, c-Src, insulin-like growth factor-1R, RET-Men2A, and RET-Men2B) or 40 μl (all other kinases) of the reaction mixture was transferred onto Immobilon-polyvinylidene difluoride membrane (Millipore, Bedford, MA), presoaked with 0.5% H_3PO_4 and mounted on a vacuum manifold. Vacuum was then applied and each well rinsed with 200 μl 0.5% H_3PO_4. Membranes were removed and washed four times with 1.0% H_3PO_4 and once with ethanol. Dried membranes were counted after mounting in a Packard TopCount 96-well frame and with the addition of 10 μl/well of Microscint. IC_{50} values ($\pm$SE) were calculated by linear regression analysis of the percentage inhibition and are averages of at least three determinations. More details of kinase assays can be found elsewhere (31, 46).

The EGFR and ErbB2 cDNAs were kindly provided by Dr. Nancy Hynes (FMI, Basel, Switzerland). Recombinant baculovirus was generated that expresses the amino acid region 668-1210 and 676-1255 of the cytoplasmic kinase domains of human EGFR and ErbB22, respectively. The coding sequence for ErbB4 kinase domain (amino acids 676-1308) was amplified by PCR from a human uterus cDNA library. For the RET kinase assay, either glutathione *S*-transferase –wild-type RET (15 ng) or glutathione *S*-transferase-RET-Men2B protein (15 ng) were used. For the Raf kinase assay, 750-1000 ng glutathione *S*-transferase-c-Raf-1 kinase was used.

Capture ELISA for Determination of ErbB2 Phosphorylation and Ligand-Induced KDR Phosphorylation. The ELISA has been developed with BT-474 cells and could also be applied to tumor lysates. BT-474 cells grown in 96-well plates (Costar #3595) close to confluency were treated for 90 min with serial dilutions of test compound (triplicates). After washing (cold PBS), cells were lysed with 150 μl/well cold lysis buffer. The lysates were either used immediately and transferred to precoated ELISA plates or stored directly in the sealed 96-well plate at −20°C. Black ELISA plates (Packard Optiplate HTRF-96) were coated with 150 ng/well anti-ErbB2 Ab2 (NeoMarkers) in 50 μl PBS overnight at 4°C. After washing (PBS/0.1% Tween; PBST; 0.1% TopBlock) and blocking (PBST; 3% TopBlock), 50 μl/well cell lysates were added and incubated for 4 h at 4°C (lysis buffer alone was included as a background control). After another washing cycle, 50 μl/well PY20(AP;0.2 μg/ml in blocking buffer) was added and incubated overnight at 4°C. The final washing cycle (3× washing buffer, 1× nanopure H_2O) was followed by incubation with 90 μl/well luminescent alkaline phosphatase substrate (CDP-Star RTU with Emerald II; TROPIX) for 45 min (dark). Luminescence was read using a Packard Top Count Microplate Scintillation Counter (Top Count). The effects of the compounds on ErbB2 phosphorylation were expressed as percentage of inhibition of the control-signal (background subtracted). Dose response curves were generated and used for determination (graphical extrapolation) of the IC_{50} values for the different compounds.

The effects of PTK787/ZK222584 were tested in a cell-based receptor phosphorylation assay using Chinese hamster ovary cells ectopically expressing human KDR and monoclonal antibody to the extracellular domain of KDR (Mab 1495.12.14) as already described (31).

ELISA for Determination of PDGF-Induced Protein Phosphorylation. A31 mouse embryonic fibroblasts, grown to 70–75% confluency in 96-well plates, were treated for 2 h (37°C) with serial dilutions of test compounds in starving medium (DMEM and 0.1% BSA). After stimulation with PDGF (50 ng/ml) for 10 min at 37°C the cells were fixed with methanol (10 min) and washed twice with PBS and once with PBST. A blocking step with PBST and 3% BSA (1 h; 37°C) was followed by incubation with 50 μl/well antiphosphotyrosine monoclonal antibody 4G10 diluted in PBST and 1% BSA (1 h; 37°C). After washing and incubation for 1 h (37°C) with AP-labeled antimouse IgG (Sigma A3688; diluted 1:1500 in PBST and 1% BSA), bound secondary antibody was detected using *p*-nitrophenyl phosphate (Sigma) as AP-substrate. Color development was measured with a Dynatec MR7000 ELISA reader at 405 nm.

Endothelial Cell Proliferation Assay. To test the effects of AEE788 on serum, VEGF, EGF, and basic fibroblast growth factor (bFGF)-induced proliferation of human umbilical vein endothelial cells an endothelial cell proliferation assay, based on BrdUrd incorporation, was used as already described previously (31).

Methylene Blue Cell Proliferation Assay and Cell Enumeration Assays. Cells were seeded at 1.5×10^3 cells/well into 96-well microtiter plates and incubated overnight at 37°C, 5% v/v CO_2 and 80% relative humidity. Two-fold serial compound dilutions were added on day 1, with the highest drug concentration being 10 μM. After incubation of the cell plates for an additional 4 (T24; BALB/ mouse epidermal keratinocyte) or 6 (BT-474, SK-BR-3, and NCI-H596) days, cells were fixed with 3.3% v/v glutaraldehyde, washed with water, and stained with 0.05% w/v methylene blue. After washing, the dye was eluted with 3% HCl and the absorbance measured at 665 nm with a SpectraMax 340 spectrophotometer (Molecular Devices, Sunnyvale, CA). IC_{50} values were determined by mathematical curve-fitting (SoftMaxPro Molecular Devices) and were defined as the drug concentration leading to 50% inhibition of net cell mass increase compared with untreated control cultures.

For the cell enumeration assay, MCF-7 and MCF-7/EGFRvIII cells were seeded (5000 cells/well) onto 24-well plates and incubated for 24 h, after which compound, vehicle, or control (no drug or vehicle) treatments were initiated. Cells were counted in a Coulter Counter (Coulter Electronics LTD, Hialeah, FL) on days 4 and 7. For 32D cells, $10–50 \times 10^9$ cells/well were seeded and treated simultaneously with compound. Fifty ng/ml of fibroblast growth factor was added to the 32D/EGFR cell culture, whereas the 32D/EGFRvIII assay was performed in the absence of EGF. Cells were counted by hemacytometry on day 2. All of the samples were prepared in triplicate.

s.c. Xenograft Models. Female BALB/c *nu/nu* (nude) mice were kept under sterile conditions (10–12 mice/type III cage) with free access to food and water. Tumors were established by s.c. injection of human NCI-H596 lung cancer cells or human prostate carcinoma DU145 cells [A431 squamous tumors for phosphorylation studies; B16 melanoma for magnetic resonance imaging (MRI) studies], respectively, into BALB/c nude mice (minimum 2×10^6 cells in 100 μl PBS). Tumors from donor mice were passaged as fragments at least three times before use. All of the treatments were initiated when a mean tumor volume of ~100 mm^3 was attained. Tumor volumes were determined according to the formula Length $\times$ $Diameter^2 \times \pi/6$. In addition to presenting changes in tumor volumes over the course of treatment, antitumor activity was expressed as T/C % (mean increase of tumor volumes of treated animals ÷ by the mean increase of tumor volumes of control animals × 100).

Genetically Engineered Mammary Gland (GeMaG) Model. HC11 mouse mammary epithelial cells were transfected with oncogenic *NeuT* and the cells (1×10^6) implanted into the cleared mammary fat pad as described previously (one gland per mouse; Ref. 45). Three to 4 weeks after transplantation, only mice showing mammary tumor growth of at least 10% during the previous 7 days were selected for efficacy studies. Animals were assigned to groups, balanced based on tumor size so that means and SE were similar in each group (10–11 animals/group). Tumor growth and body weights were determined twice per week.

Statistical Analyses. When applicable, results are presented as mean ± SE. For statistical analysis of antitumor effects the change in tumor volume was used. These were found to be normally distributed, and comparison of the groups used one-way ANOVA with post-hoc Dunnett's test to compare the treated groups with the controls and Tukey's test to perform pair-wise comparisons. Differences in the body weights within treatment groups, between the start of treatment and the end of treatment, were analyzed by paired *t* tests and between groups by Kruskal-Wallis ANOVA on ranks and Dunn's test for not normally distributed data; first experiment) or one-way ANOVA and Dunnett's or Tukey's test (for normally distributed data; second experiment) using the change in body weight. For all of the tests the level of significance was set at $P < 0.05$. Statistical calculations were performed using SigmaStat 2.0 (Jandel Scientific).

***In Vivo* Growth Factor-Induced Angiogenesis Model.** VEGF-mediated angiogenesis was tested in comparison with PTK787/ZK222584 in a growth factor implant model in mice as described previously (31). To test the specificity of the response, the effects on bFGF-induced angiogenesis were also tested. We have shown previously that these growth factors induce dose-

dependent increases in weight and blood content of the tissue growing (characterized histologically to contain fibroblasts and small blood vessels) around the chambers and that this response is blocked by antibodies that specifically neutralize the growth factors (31).

Tumor Extract Preparation, Immunoprecipitation, and Immunoblotting. BALB/c mice bearing s.c. A-431 squamous tumors (3 animals/group) or HC11-NeuT-driven breast tumors (2 animals/group) were dosed orally with 30 mg/kg of AEE788 or vehicle once daily for 5 days. At different time points after the end of compound treatment and before sacrificing the animals the mice were given i.v. 500 μg EGF/kg body weight or 0.2 ml 0.9% w/v NaCl as vehicle control. Five min after EGF administration, the mice were sacrificed, tumors were removed, dissected free of necrotic material, snap-frozen in liquid nitrogen, and stored at −80°C. Tumors were homogenized at 4°C for 15 s in 10 volumes of lysis buffer using an Ultra-Turrax (Model T25). After 30-min incubation on ice, lysates were cleared by centrifugation in an Eppendorf centrifuge (14,000 rpm for 10 min at 4°C) and stored at −70°C. Lysates were diluted 1:2000 with H_2O for determination of protein concentrations using BSA as a standard (Pierce; Cat. No. 23236 and 23209), and adjusted to a total protein concentration of 200 μg/ml in lysis buffer. Lysates were used directly for determination of receptor phosphorylation or in serial dilutions in lysis buffer for the determination of relative EGFR amounts.

For immunoprecipitation, lysates were adjusted to a volume of 400 μl containing 400 μg of total protein and incubated with 2.5 μg (10 μl) anti-hu-EGFR monoclonal antibody for EGFR detection. After 2-h incubation at room temperature, 75 μl of protein A-Sepharose beads (Sigma P-9424) were added followed by overnight incubation (with gentle shaking) at 4°C. Immunoprecipitates were washed twice with cold PBS, resuspended in 60 μl of 2× concentrated sample buffer, heated for 10 min to 70°C, and analyzed by immunoblotting as described below. For ErbB2, the procedure was the same as above but using an anti-ErbB2 antibody.

For immunoblotting, immunoprecipitates were subjected to 7.5% w/v SDS PAGE analysis, and proteins were transferred onto a polyvinylidene difluoride membrane (Millipore) by semidry electroblotting (90 min at 0.8 mA/cm^2). Membranes were blocked with 5% (w/v) milk powder in PBST for 1 h at room temperature then probed with antiphosphotyrosine antibodies (0.5 μg/ml) for 2–4 h at room temperature or overnight at 4°C. Bound antibodies were visualized with horseradish peroxidase-coupled secondary antibodies using the enhanced chemiluminescence detection system from Amersham (Buckinghamshire, United Kingdom). Filters were stripped in a buffer containing 62.5 mM Tris-HCl (pH 6.7), 2% (w/v) SDS, and 100 mM β-mercaptoethanol for 30 min at 60°C; washed three times, and incubated in Tween Tris-buffered saline (TTBS) (2 × 10 min). Membranes were blocked and reprobed with an antihuman EGFR (1:750) or anti-ErbB2 antibody, and bound antibodies were detected using the appropriate secondary antibody.

Pharmacokinetics in Tumor-Bearing and Normal Mice. Female athymic tumor-bearing mice (human adenosquamous lung carcinoma NCI-H596 with tumors ~250 mm^3) or normal mice received an oral dose of 100 mg/kg of AEE788 [formulated in *N*-methylpyrrolidone/PEG300 (10%/90% v/v) by gavage]. At the allotted time points, mice (n = 4) were sacrificed, blood and tissues (tumor, liver, and muscles) removed, and processed as below.

For preparation of plasma, tumor, and tissue samples, proteins were precipitated by the addition of an equal volume of acetonitrile for 20–30 min at room temperature, the protein precipitate was recovered by centrifugation (10,000 × g; 5 min), and 1 ml/gram tissue of PBS [137 mM NaCl, 2.7 mM KCl, and 10 mM phosphate buffer(pH 7.4); Sigma P4417] was added. Tissues were homogenized on ice using an ULTRA-TURRAX (TP18–10; IKA, Staufen, Germany) homogenizer (15-s bursts). Proteins in the homogenate were precipitated by the addition of an equal volume of acetonitrile. After 20–30 min at room temperature, the protein precipitate was removed by centrifugation (10,000 × g; 5 min). The obtained supernatants were analyzed immediately by reversed-phase high-performance liquid chromatography.

High-performance liquid chromatography analysis was carried out using Merck-Hitachi LaChrom equipment. The deproteinated samples were injected (100 μl) onto a Nucleosil 100–5 C18 column (125 × 4.6 mm; with an 8 mm guard column of the same material) equilibrated with 10% v/v acetonitrile in water containing 0.05% v/v trifluoroacetic acid at a temperature of 30°C. The sample was eluted with a linear gradient of 10–90% v/v acetonitrile in water containing 0.05% v/v trifluoroacetic acid over a period of 20 min at 1 ml/min. The compounds were detected by UV absorbance (320 nm) and concentrations determined by the external standard method using peak heights. The calibration curve was obtained from known concentrations of compound added to plasma or tumor homogenates obtained from untreated animals and processed in the same way. The limit of quantitation was 0.1–0.2 μM in plasma and 0.2–0.4 nM/g in tissues. Mean values and SE are calculated from four individual mice for each time point.

B16/BL6 Orthotopic/Syngeneic Melanoma Model for Efficacy and Dynamic Contrast Enhanced (DCE)-MRI Studies. B16 melanoma cells were injected in both ears of female black C57 BL6 syngeneic mice weighing 20–25 g. For efficacy experiments, animals (n = 6) were dosed with AEE788 (50 mg/kg; p.o.) or vehicle once daily from day 8 to 21 after tumor cell inoculation, and the surface area of the primary tumor was determined every 7 days. All of the animals were sacrificed after 21 days, and the regional (cervical) lymph node metastases were resected and weighed. Cervical metastases were also examined by DCE-MRI after at least 14 days of growth. Directly after the first MRI, PTK787/ZK222584 (100 mg/kg, p.o.; n = 6), AEE788 (50 mg/kg, p.o.; n = 6), or vehicle (n = 4) were administered by gavage (10 ml/kg) daily for another 3 days including the day of the second MRI examination (treatment 2 h before the second MRI scan).

Mice were anesthetized using 1.5% isoflurane (Abbott, Cham, Switzerland) in a 1:2 mixture of O_2:N_2O and placed on an electrically warmed pad for cannulation of one of the two tail veins using a 30-guage needle attached to an infusion line of 30 cm and volume 80 μl to permit remote administration of the contrast agent. The animals were positioned on a cradle in a supine position inside the 30-cm horizontal bore magnet and were anesthetized with 1.5% isoflurane in a 1:2 mixture of O_2:N_2O administered with a face mask (flow-rate: 0.7 liter/min). The mouse body temperature was maintained at 37 ± 2°C (monitored with rectal probe). DCE-MRI experiments were performed on a Bruker DBX 47/30 spectrometer (Bruker BioSpin AG, Fällanden, Switzerland) at 4.7T equipped with a self-shielded 12-cm bore gradient system as described previously (47). The contrast agent GdDOTA (Dotarem) was injected (30 μl) as a bolus during dynamic image acquisitions for determination of tumor vascular permeability (VP) and extravasion, *i.e.*, tumor cell interstitial leakage space (LS), and similarly ~15 min later 60 μl of the iron oxide particle intravascular contrast agent, ENDOREM, was injected for determination of tumor relative blood volume. The principles behind measurement of these parameters have already been described (47). In addition, the first 20 points (102 s) from the injection of GdDOTA were used to calculate the area under the enhancement curve for the increase in relative Gd^{2+} concentration, which had been used to determine the initial slope *i.e.*, permeability (VP) and plateau value *i.e.*, interstitial LS. This calculation gave an additional parameter, the GdDOTA area under the enhancement curve, which was equivalent to that used in the clinical analyses by Morgan *et al.* (48) for PTK787/ZK222584.

Table 1 *In vitro profile of AEE788 against a panel of kinases*

Kinase	IC_{50} [μM] ± SE[a]
EGFR ICD[b]	0.002 ± 0.0006
ErbB2 (HER-2)	0.006 ± 0.0006
ErbB4 (HER-4)	0.16 ± 0.026
KDR	0.077 ± 0.009
Tek	2.1 ± 0.32
IGF1-R	>10
Ins-R	>10
PDGFR-β	0.32 ± 0.038
c-Met	2.9 ± 0.38
c-Abl	0.052 ± 0.010
c-Src	0.061 ± 0.013
c-Kit	0.79 ± 0.094
RET	0.74 ± 0.03
c-Fms	0.060 ± 0.005
Flt-1	0.059 ± 0.009
Flt-3	0.73 ± 0.12
Flt-4	0.33 ± 0.099
Cdk1/Cyc.B	8.0 ± 0.79
PKC-α	>10
c-Raf-1	2.8 ± 0.49
PKA	>10

[a] Results are expressed as means ± SE; all values are averages of at least three determinations.

[b] EGFR ICD, cloned and purified epidermal growth factor receptor intracellular domain; IGF, insulin-like growth factor; PDGFR, platelet-derived growth factor receptor; Cdk, cyclin-dependent kinase; PKC, protein kinase C; PKA, protein kinase A.

Table 2 *Effects on ligand-induced phosphorylation in cell-based ELISA assays*[a]

Compound	EGFR[b]	ErbB2	KDR	PDGFR
	A431 cells	BT-474 cells	CHO cells	A31 cells
		IC_{50} [μM] ± SE		
AEE788	0.011 ± 0.05	0.22 ± 0.04	0.96 ± 0.25	> 10
	$n = 3$	$n = 9$	$n = 6$	$n = 3$

[a] Mean ± SE, n = number of experiments.
[b] EGFR, epidermal growth factor receptor; PDGFR, platelet-derived growth factor receptor; CHO, Chinese hamster ovary.

Table 3 *Antiproliferative activity of AEE788*

Cell line	IC_{50} [μM]
NCI-H596[a]	0.078 ± 0.044
MK[a]	0.056 ± 0.011
BT-474[a]	0.049 ± 0.005
SK-BR-3[a]	0.381 ± 0.028
32D/EGFR[b]	~0.300
32D/EGFRvIII[b]	0.010
MCF-7[b]	2.5
MCF-7/EGFRvIII[b]	<5
T24[a]	4.526 ± 0.305

[a] IC_{50} values are presented as mean ± SE of at least three experiments.
[b] Coulter Counter assay (two experiments, performed at Lombardi Cancer Center, Georgetown University Medical Center, Washington, DC).

In all of these experiments, animals were checked daily, and any animals visibly suffering from the effects of the metastases (lymph node or lung) were sacrificed.

RESULTS

Inhibition Profile of AEE788 against Purified Protein Kinases *in Vitro*. The *in vitro* profile of AEE788 against a panel of tyrosine and serine/threonine kinases is shown in Table 1. AEE788 potently inhibited the EGFR/ErbB2 tyrosine kinases (IC_{50}: 2 nM and 6 nM, respectively) as well as KDR (IC_{50}: 77 nM). The compound also inhibited c-Abl, c-Src, and Flt-1 tyrosine kinases with similar IC_{50} values as obtained for KDR inhibition, but only weakly inhibited ErbB-4, PDGF receptor-β, Flt-3, Flt-4, RET, and c-Kit tyrosine kinases (IC_{50}s: 160 nM, 320 nM, 720 nM, 330 nM, 740 nM, and 790 nM, respectively). AEE788 did not inhibit the Ins-R, insulin-like growth factor-1R, protein kinase C-α, and cyclin-dependent kinase 1/cyclin B kinases.

Inhibition of Ligand-Induced Phosphorylation and Proliferation in Cell Cultures. The effect of AEE788 on EGFR, ErbB2, and KDR phosphorylation, as well as PDGF-induced cellular protein phosphorylation, was measured using cell-based ELISAs (Table 2). AEE788 potently inhibited EGFR phosphorylation in A431 cells in the low nM range (IC_{50}: 11 nM). Phosphorylation of KDR in Chinese hamster ovary cells and ErbB2 in BT-474 cells was also inhibited in the submicromolar range. As expected, PDGF-induced phosphorylation was unaffected.

The antiproliferative activity of AEE788 was also tested using growth factor-dependent cell proliferation assays. The cellular model systems used were mouse keratinocytes and NCI-H596 (human lung squamous adenocarcinoma) cells, which express or overexpress the EGFR, respectively, and BT-474 (human mammary gland ductal carcinoma) and SK-BR-3 (human breast adenocarcinoma) cells that overexpress ErbB2. As an indicator for selectivity, the compound was also tested in T24 bladder carcinoma cells (Ras transformed), which proliferate independently of ErbB signaling and, consequently, should not be affected by EGFR/ErbB2 inhibitors. As shown in Table 3, AEE788 potently inhibited the proliferation of the two EGFR-expressing cell lines (IC_{50}: 56 nM and 78 nM, respectively) as well as the ErbB2-overexpressing cell lines (IC_{50}: 49 nM and 381 nM, respectively). These data suggest that the candidate effectively targets the ErbB receptors at the cellular level. As expected, AEE788 displayed a considerably higher IC_{50} value against T24 cells (IC_{50}: 4.5 μM), suggesting selective growth inhibition of cells overexpressing EGFR/ErbB2. Additional analyses using human umbilical vein endothelial cells demonstrated that AEE788 further inhibited both EGF- and VEGF-driven proliferation in the nanomolar range (IC_{50}s: 43 nM and 155 nM, respectively) with no effect on either serum or bFGF-induced proliferation at concentrations of up to 1 μM (Table 4). Taken together, these data demonstrate the potency of AEE788 for both ErbB receptor- and VEGF-driven cell proliferation. However, the analysis was taken further to include the EGFRvIII mutant, a constitutively activated ligand-independent oncoprotein, which plays an important role in the pathogenesis of breast cancer. AEE788 also inhibited anchorage-dependent EGFRvIII-mediated proliferation in EGFRvIII-expressing cells (32D/EGFRvIII) with IC_{50}s in the low nM range (IC_{50}: 10 nM; Table 3). In addition, the compound blocked EGFRvIII phosphorylation in MCF7/EGFRvIII cells (data not shown). Hence, AEE788 has the additional property of inhibiting cellular proliferation driven by this clinically relevant EGFR mutant.

Pharmacokinetic Characteristics of AEE788 in Tumor-Bearing and Normal Mice. To assess the pharmacokinetic characteristics of AEE788 in mice, plasma drug levels and disposition of AEE788 to tumor, muscle, and liver were studied in athymic NCI-H596 tumor-bearing nude mice. The mean plasma and tumor concentrations of AEE788 after oral administration of a single 100 mg/kg oral dose of AEE788 are shown in Fig. 2. The pharmacokinetic parameters derived

Table 4 *Effect of AEE788 on HUVEC*[a] *proliferation Proliferation assays based on BrdUrd incorporation were performed with endothelial cells (HUVECs) in 96-well plates with 5 × 10^3 cells per well using FCS (5%) or VEGF, EGF, or bFGF (in the presence of 1.5% FCS) to stimulate the cells in the absence or presence of increasing concentrations of AEE788. Data given are from three independent experiments and represent IC_{50} as well as the mean ± SE from all of the experiments.*

VEGF-stimulated	EGF-stimulated	BFGF-stimulated	FCS-stimulated
IC_{50} (μM) ± SE	IC_{50} (μM) ± SE	IC_{50} (μM) ± SE	IC_{50} (μM) ± SE
0.155 ± 0.02	0.043 ± 0.034	3.61 ± 1.92	5.18 ± 1.76

[a] HUVEC, human umbilical vascular endothelial cell; BrdUrd, bromodeoxyuridine; VEGF, vascular endothelial growth factor; EGF, epidermal growth factor; bFGF, basic fibroblast growth factor.

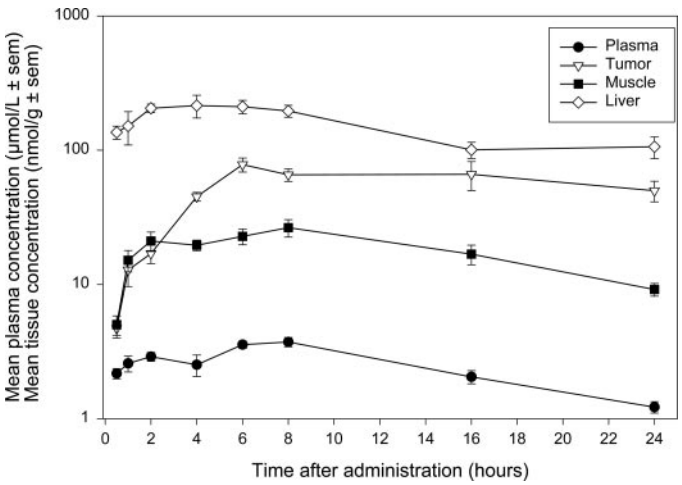

Fig. 2. Plasma, tumor, and tissue concentrations of AEE788 in tumor-bearing mice after a single oral dose of 100 mg/kg. Female athymic nude mice bearing s.c. xenotransplants of the human adenosquamous lung carcinoma NCI-H596 of ~250 mm^3 received a dose of 100 mg/kg AEE788 formulated in *N*-methylpyrrolidone/PEG300 (10%/90% v/v) by gavage. At the allotted times, the groups of mice ($n = 4$) were sacrificed, blood and tissues removed, and the concentration of the compound determined by reversed-phase high-performance liquid chromatography-UV analysis. *Bars*, ±SE, $n = 4$. To convert to ng/ml or ng/g multiply by 440.6.

Table 5 *Pharmacokinetic parameters for AEE788 in plasma, tumor, and normal tissues after oral administration of 100 mg/kg to tumor-bearing mice*

Parameter[a]	Sample matrix			
	Plasma	Tumor	Muscle	Liver
t_{max} (h)	8.0	6.0	8.0	4.0
t_{last} (h)	24.0	24.0	24.0	24.0
C_{max} (μmol/l or nmol/g)	3.73 ± 0.30	78.13 ± 9.34	26.40 ± 3.96	241.90 ± 41.17
C_{last} (μmol/l or nmol/g)	1.22 ± 0.12	49.96 ± 8.72	19.17 ± 1.0	106.05 ± 19.45
$AUC_{(0.5–24\ h)}$ (h·μmol/l or h·nmol/g)	58.50	1337.31	428	3508

[a]Areas under the curve (AUC) were calculated by noncompartmental analysis of extravascular dosing (WinNonlin) using mean values. Cmax (maximum concentration) and tmax (time to maximum concentration) were determined by inspection of the data. Data are expressed as mean ± SE (n = 4).

from these data are summarized in Table 5. AEE788 appeared rapidly in the circulation attaining a concentration maximum of 3.73 ± 0.3 μmol/liter at 8 h. The terminal pharmacokinetics of AEE788 were characterized by a slow elimination phase with a concentration of 1.22 μmol/liter at 24 h. The concentration *versus* time profile of AEE788 in tumor and normal tissues after a single oral dose of 100 mg/kg revealed a substantially higher exposure than that found in plasma. In tumor tissue the apparent concentration maximum was 78.13 ± 9.34 nmol/g at 6 h. This amount corresponded to ~20-fold the concentration found in plasma. The drug was more slowly eliminated from the tumor tissue as compared with plasma. After 24 h, the concentration in tumors was ~50 nmol/g. This level corresponded to ~60% of the concentration maximum at 6 h. The pharmacokinetic profile for muscle and liver was similar to that found for tumor tissue; however, compound levels in liver were ~3-fold higher than those found in tumor tissue, whereas the levels in muscle were approximately three times lower. The high exposure of tumor tissue to AEE788 was also reflected by the high area under the curve from 0.5h to 24 h of 1337 h·nmol/g.

In normal mice the pharmacokinetic profile in plasma exhibited similar characteristics as found in tumor-bearing athymic nude mice. Specifically, after oral dosing with 30 and 10 mg/kg of AEE788, a dose-proportional relationship was observed in plasma and muscle, and terminal half-lives ranged from 8 h in plasma to 11 h in muscle (data not shown).

Antitumor Efficacy of AEE788 in Relevant Disease Models. In nude mice, the acutely tolerated dose using a single oral administration was >100 mg/kg. The maximally tolerated dose (12 consecutive daily oral administrations) was 30 mg/kg. In normal mice, AEE788 appeared to be better tolerated (data not shown).

On the basis of this information, AEE788 treatment schedules were selected to evaluate the antitumor efficacy of AEE788. For this, three relevant mouse tumor models were used: (*a*) the EGFR-overexpressing NCI-H596 adenosquamous lung carcinoma xenograft model; (*b*) the ErbB2-driven syngeneic orthotopic *NeuT*/GeMag tumor model (45); and (*c*) the DU145 human prostate carcinoma xenograft model.

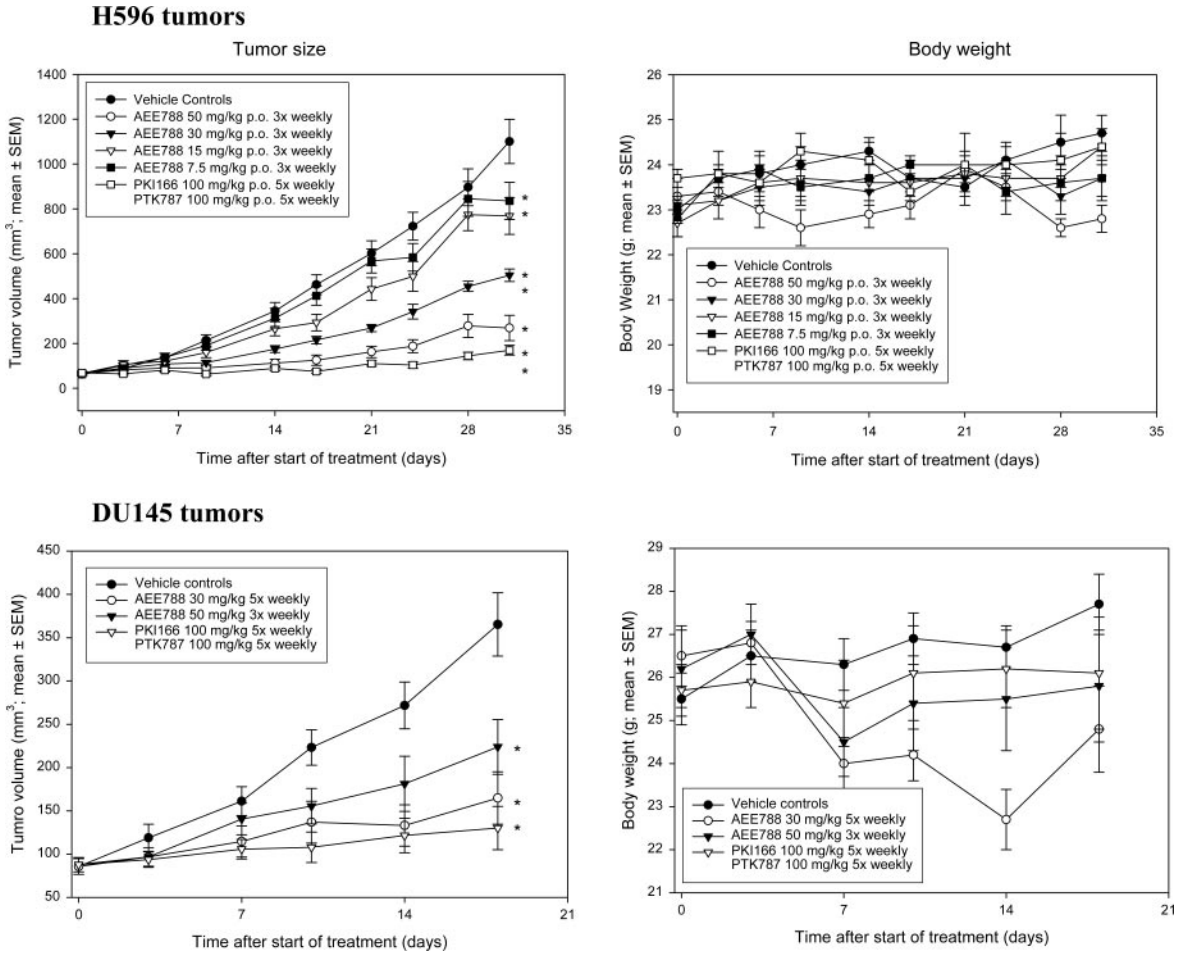

Fig. 3. Effect of AEE788 in the mouse xenografts models NCI-H596 and DU145 H596 tumors. Tumor fragments (~40 mm^3) were implanted s.c. into BALB/c nude mice. Treatment was started when tumor volumes had reached ~100 mm^3 (10 days after tumor implantation for H596; 31 days for DU145). AEE788 was given three times or five times per week at the dose indicated. In the combination of PKI166 and PTK787, both compounds were given five times weekly at 100 mg/kg. Tumor volumes and body weights were determined twice per week. *, $P < 0.05$ *versus* controls (ANOVA and Dunnett's test).

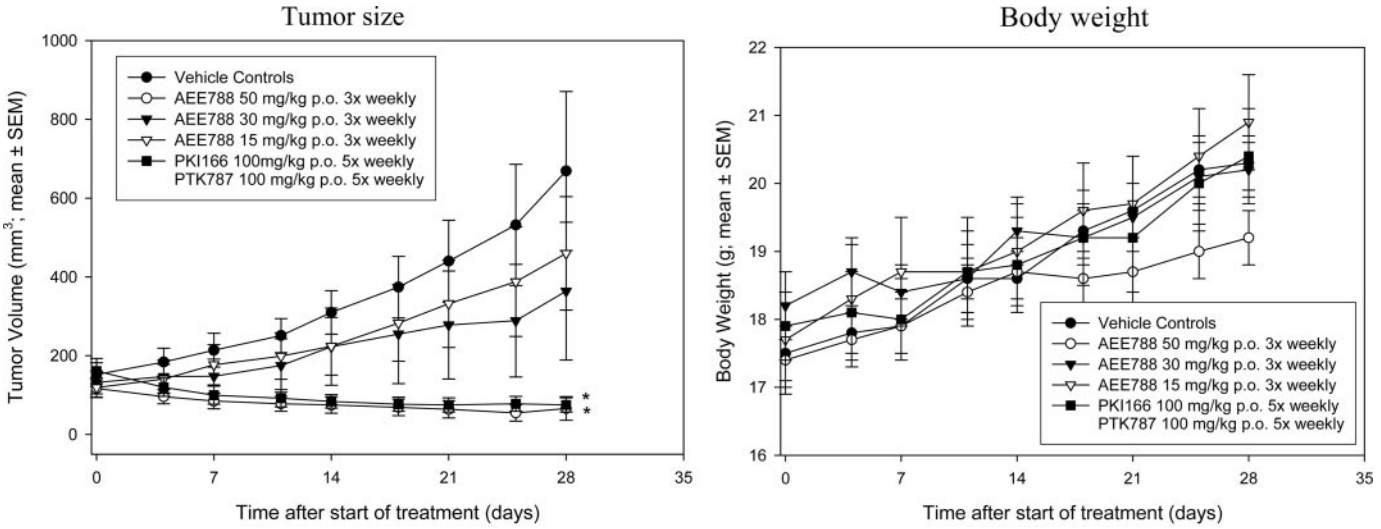

Fig. 4. Effect of AEE788 in the ErbB2-driven *NeuT*/ErbB2 genetically engineered mammary gland tumor model. HC11 cells were transfected with *neu*T, and 1×10^6 cells were inoculated into the 4th cleared mammary fat pad of female BALB/c mice. After 3–4 weeks the tumors became palpable. Only mice showing at least 10% increase in tumor volume over the previous 7 days were selected and randomized into groups balanced for tumor size. Treatment was started on the day of randomization. AEE788 was given three times per week. PKI166 and PTK787/ZK222584 were given in combination five times per week at the dose indicated. Tumor volumes and body weights were determined twice per week. *, $P < 0.05$ *versus* controls (ANOVA on ranks and Dunnett's test on ratio of final tumor volume to initial tumor volume); *bars*, ±SD.

The latter tumor is well vascularized and known to respond to both EGFR and VEGFR inhibitors. In all of the cases, a combination of the EGFR inhibitor PKI166 (5, 42) plus the VEGFR inhibitor PTK787/ZK222584 (7, 31) was used as a reference.

In the NCI-H596 xenograft model, three-times weekly oral application of AEE788 produced a dose-dependent inhibition of s.c. tumor growth (Fig. 3). Moreover, at the highest dose of 50 mg/kg, the activity of AEE788 was similar to that obtained with a combination of PKI166 and PTK787/ZK222584, where 100 mg/kg of each compound was given five times per week. Specifically, T/C values after 31 days treatment were 20% and 10%, respectively. Treatment with AEE788 was associated with only minor body weight changes. Splitting the same total dose of 150 mg/kg of AEE788 into 5, 3, 2, or 1 administrations per week produced similar growth inhibition, with T/C values after 17 days ranging from 18% to 35%. All of these treatments were well tolerated with at worst <10% body weight loss (data not shown).

In the DU145 prostate carcinoma model, the efficacy of AEE788 was evaluated using oral doses of 50 mg/kg, administered three times per week, or 30 mg/kg, administered five times per week. In two experiments, the daily regimen provided slightly better results (T/C of 28 and 27% at the end of treatment) than the three-times weekly experiment (T/C of 57% and 49% at the end of treatment). Again, AEE788 single-agent activity was comparable with the PKI166 and PTK787/ZK222584 combination, and there was no associated statistically significant decrease in body weights (Fig. 3).

In the *NeuT*/ErbB2 GeMag model, a *NeuT* (a constitutively active rat mutant ErbB2)-overexpressing HC11 mammary epithelial cell subline was used to develop an orthotopic, ErbB2-driven tumor model. The majority of mammary fat pads of BALB/c syngeneic mice injected with HC11-*NeuT* cells develop tumors, which appear after a 3 ± 4-week latency period and, subsequently, grow rapidly. Non-transfected HC11 cells fail to produce tumors (45). Using this model, three times weekly oral administration of 15, 30, and 50 mg/kg of AEE788 produced a dose-dependent inhibition of tumor growth suggestive of a particular sensitivity of this ErbB2-driven model to AEE788 treatment. There was a clear trend to regression (57% tumor regression with the highest dose), which was statistically significant (*t* test). AEE788 was again well tolerated (Fig. 4), and the dose-dependency was fully confirmed in a second experiment (data not shown). At the highest dose of 50 mg/kg, the activity of AEE788 was similar to that of the combination of PKI166 and PTK787/ZK222584, where 100 mg/kg of each compound was given five times per week (44). Splitting the same total dose of 150 mg/kg AEE788 into 5, 2, or 1 administrations per week produced similar effects in this model. All three of the regimens gave strong inhibition of tumor growth with T/C values of 6%, 12%, and 1%, respectively, and were well tolerated (data not shown).

Taken together, these data illustrate that AEE788 is a potent antitumor agent in a number of ErbB-driven animal models of human cancer. Importantly, AEE788 elicited a similar antitumor response as the combined administration of an ErbB inhibitor with a VEGFR inhibitor, additionally illustrating the dual activity of this inhibitor.

Inhibition of EGFR/ErbB2 Phosphorylation in Tumors. Analysis of EGFR and ErbB2 phosphorylation levels in tumor tissue was used to correlate the antitumor effects of AEE788 with a pharmacodynamic marker of drug action. For the EGFR phosphorylation studies, nude mice bearing human EGFR-overexpressing A431 epidermoid carcinomas were treated for 5 days with 30 mg/kg AEE788 (p.o.). Because A431 tumors demonstrate only a low basal level of phosphorylated EGFR, animals were additionally challenged with 0.5 μg EGF/g body weight given by i.v. administration at the indicated time-points after last administration. After 5 min, the animals were sacrificed, and the EGFR phosphorylation status of the tumor was analyzed by immunoblotting and by a capture ELISA assay.

ErbB2 phosphorylation was also assessed using samples from the above-mentioned A431 tumors and also from GeMag tumors. For the latter, mice bearing these GeMag tumors were treated for 5 days with 30 mg/kg of the compound. At the indicated time-points after last administration, the animals were challenged with i.v. administration of 0.5 μg EGF/g body. After 5 min, the animals were sacrificed and the ErbB2 phosphorylation status of the tumor analyzed by immunoblotting.

The data show that AEE788 potently inhibited EGF-induced EGFR phosphorylation in A431 tumors up to 72 h after the last administration, with the signal returning to control levels after 96 h (Fig. 5*A*). Importantly, no effect of administration of vehicle alone was observed (Fig. 5*B*). EGFR levels remained practically unchanged under treatment with AEE788 (data not shown). An additional experiment,

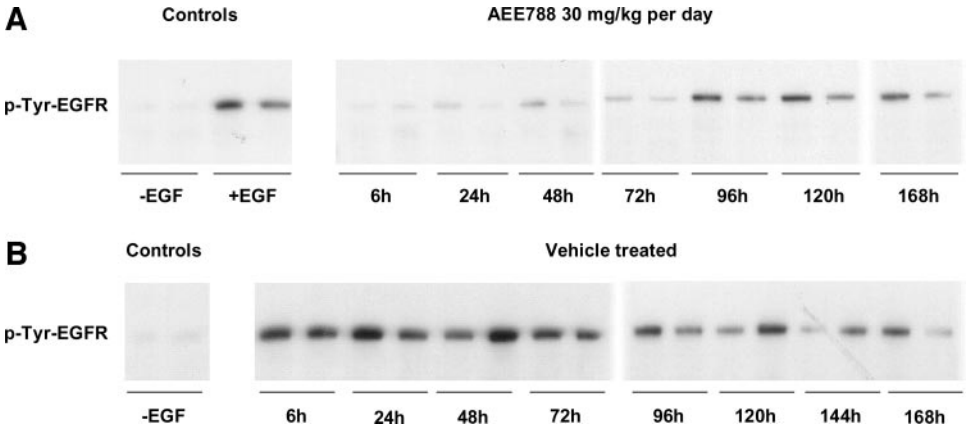

Fig. 5. Inhibition of epidermal growth factor (*EGF*)-induced phosphorylation of the epidermal growth factor receptor (*EGFR*) by AEE788 in A431 tumor xenografts. A431 tumor-bearing nude BALB/c mice were treated daily for 5 days with 30 mg/kg AEE788 (*A*) or vehicle (*B*), and, at the times indicated after last dose, 0.5 μg/g body weight EGF was administered, and 5 min later animals were sacrificed and tumors removed. For detection of EGFR phosphorylation, 400 μg of total tumor lysates were precipitated with a mouse monoclonal antihuman EGFR-antibody. An aliquot was resolved by SDS-PAGE and blotted onto a polyvinylidene difluoride membrane. The membrane was then incubated with a monoclonal anti-human-pTyr antibody. Phosphorylated EGFR (*p-Tyr-EGFR*) was then visualized with anti-mouse-IgG using enhanced chemiluminescence technology. Controls represent tumors derived form untreated animals (±EGF administration).

where the tumors were analyzed by a capture ELISA, gave similar results (data not shown). As expected and illustrated in Fig. 6, EGF stimulation did not dramatically affect ErbB2 phosphorylation in A431 tumors as assessed by capture ELISA. In tumors from compound-treated mice, however, ErbB2 phosphorylation was dramatically reduced to near-assay background levels already after 6 h. This inhibitory effect lasted for up to 72 h after drug administration (the last time point analyzed in this experiment). Similarly, in GeMag tumors AEE788 potently inhibited ErbB2 phosphorylation for at least 24 h, as compared with both EGF-stimulated and nonstimulated tumors (Fig. 7). ErbB2 protein levels remained unchanged after treatment with the compound. In this model, a reduction in the phosphorylation of ErbB2 was observed after stimulation with EGF, an effect that has been observed previously in other ErbB2-overexpressing tumor lines, and which to date is not fully understood. Consistent with these data, immunoblot analysis of tumor samples from the efficacy studies in H-596 tumors also showed inhibition of EGFR and ErbB2 phosphorylation for >72 h after 4 weeks of treatment (data not shown).

These phosphorylation analyses indicate that AEE788 treatment has long-term effects on ErbB receptor signaling in tumor, an observation consistent with the efficacy of intermittent treatment schedules and with the high and prolonged tumor exposure observed with this agent.

Antiangiogenic Effects of AEE788 in a Growth Factor Implant Mouse Model. s.c. implants containing VEGF or bFGF in normal mice induce the growth of vascularized tissue around the implant. This response is concentration dependent, can be quantified by measuring the weight and the amount of hemoglobin (blood content) in the tissue, and can be specifically blocked by selective inhibitors of endothelial cell growth factors and their signaling pathways. Indeed, this model was successfully used to characterize the antiangiogenic properties of PTK787/ZK222584 (7, 31). Consequently, this model was used to evaluate the antiangiogenic properties of AEE788 using PTK787/ZK222584 as a comparator compound and PKI166 as a negative control. AEE788 dose-dependently inhibited angiogenesis induced by VEGF with ED_{50}s from two experiments of 26 and 32 mg/kg, respectively, similar to those obtained with PTK787/ZK222584 (ED_{50}s: 29 and 42 mg/kg; Table 6). In agreement with *in vitro* data (Table 4), AEE788 did not inhibit bFGF-induced angiogenesis in this model (Table 6). Hence, AEE788 exhibits a similar potency as PTK787/ZK222584 in terms of inhibition of VEGFR-induced angiogenesis in this model. As expected, the EGFR/ErbB2 inhibitor PKI166 was inactive in this model (Table 6).

Antiangiogenic Effects of AEE788 as Measured by DCE-MRI. Antiangiogenic activity can be detected noninvasively using DCE-MRI. This primarily monitors tumor VP and interstitial LS but also tumor blood-flow index and relative tumor blood volume (relative blood volume). This approach has been successfully used to demonstrate the antiangiogenic activity of PTK787/ZK222584 using the B16/BL6 melanoma metastatic mouse model. Specifically, VEGFR inhibition was observed to decrease both VP and LS, and the associated area under the enhancement curve, in the cervical lymph nodes 2–4 days after initiation of daily treatment with PTK787/ZK222584.[4] PTK787/ZK222584 also induced a decrease in VP in an experimental renal tumor (47). Using the B16/BL6 model, AEE788, given 8–21 days after cell inoculation at a daily dose of 50 mg/kg, reduced the size of the primary tumors by 64% and the size of cervical lymph nodes by 70% (data not shown). Moreover, MRI analysis of animals with established tumors (2–3 weeks old) demonstrated that daily oral treatment for 3 days with 50 mg/kg AEE788 significantly decreased the area under the enhancement curve by 34 ± 10%, whereas vehicle had no significant effect (6 ± 19%; Fig. 8*A*). The decrease induced by AEE788 was very similar to that observed for PTK787/ZK222584 administered at 100 mg/kg (29 ± 12%). There was a trend for the individual parameters of VP and LS to decrease (20–30%), but this only reached significance on LS for AEE788 (results not shown). Both AEE788 and PTK787/ZK222584 also reduced relative blood volume by 36% ± 8% and 30% ± 4%, respectively. The vehicle also showed this trend (−28% ± 8%), although not reaching significance (Fig. 8*B*). In conclusion, the effects on the vasculature of B16/BL6 cervical tumors as measured by DCE-MRI are also consistent with an antiangiogenic activity of AEE788.

DISCUSSION

There is accumulating evidence from the literature that combined blockade of both EGFR and VEGFR signal transduction pathways might lead to beneficial clinical effects (41). We have demonstrated previously in two mouse models that concomitant administration of the EGFR/ErbB2 tyrosine kinase inhibitor PKI166 with the VEGFR tyrosine kinase inhibitor PTK787/ZK222584 (Phase III) has additive/synergistic effects on tumor growth (44). Through optimization of the pyrrolo[2,3-*d*]pyrimidine lead scaffold, we have now obtained AEE788, a compound that combines EGFR/ErbB2 as well as VEGFR tyrosine kinase inhibition in the same molecule. When profiled as an inhibitor of the ErbB family of tyrosine kinases, AEE788 inhibited both the EGFR and ErbB2 enzymes with low nanomolar IC_{50} values. In cell-based ELISAs, ligand-induced EGFR phosphorylation in A431 cells or ErbB2 phosphorylation in BT-474 was also affected in the low nM and submicromolar range, respectively. The demonstrated potent

[4] M. Rudin, P. M. J. McSheehy, P. R. Allegrini, D. Baumann, M. Bequet, K. Brecht, S. Ferretti, F. Schaeffer, C. Schnell, and J. Wood, manuscript in preparation.

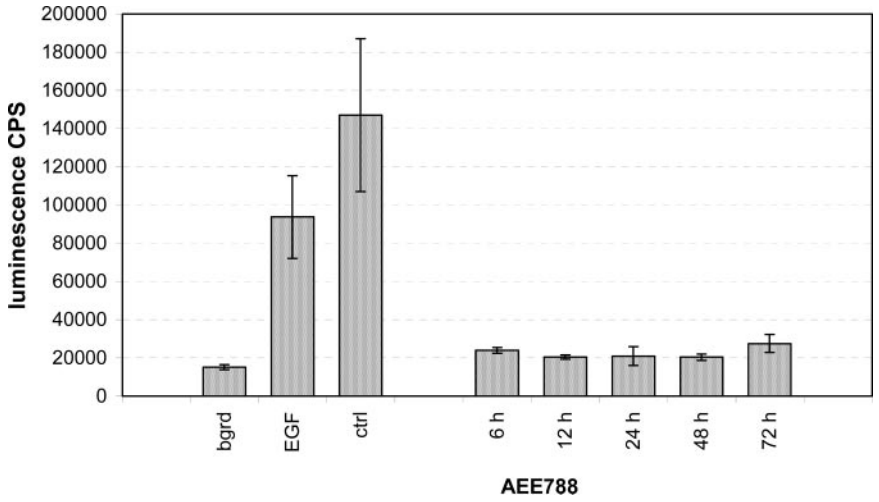

Fig. 6. Inhibition of ErbB2 phosphorylation by AEE788 in A431 tumor xenografts *in vivo*. Tumor lysates were prepared as described in Fig. 5. ErbB2 phosphorylation was examined in a capture ELISA using anti-ErbB2 Ab2 (Neomarkers) as coating antibody and PY20 alkaline phosphatase (AP), an anti-P-tyr antibody labeled with AP, as a second antibody. Ten μg total tumor lysate protein per were added to the ELISA plate in triplicates. ErbB2-phosphorylation was determined via binding of PY20 (AP) to the captured receptors and measured with a luminescent substrate (CDPStar RTU with Emerald II). Luminescence was read as counts per second with a Packard TopCount. Each group contained three tumor samples. The means for each group are shown; *bars*, $\pm$SD. *bgrd*, background measurement without lysate; *ctrl* and *EGF*, ErbB2 phosphorylation levels before and after epidermal growth factor administration, respectively.

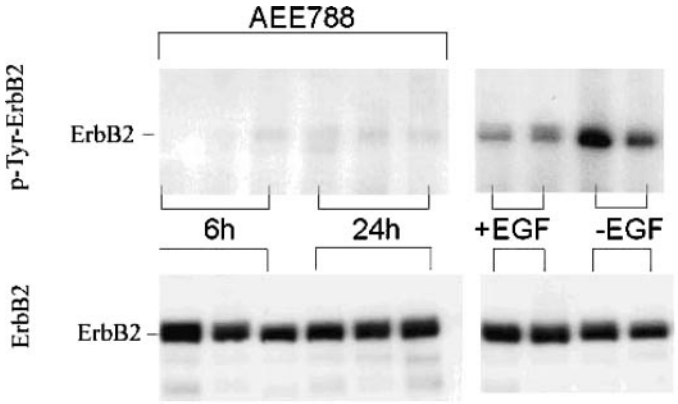

Fig. 7. Inhibition of ErbB2 phosphorylation by AEE788 in genetically engineered mammary gland tumors *in vivo*. Female BALB/c mice bearing genetically engineered mammary gland tumors were treated daily for 5 days with 30 mg/kg AEE788. At the indicated times after last administration, 0.5 μg/g body weight epidermal growth factor (*EGF*) was administered, and 5 min later animals were sacrificed and tumors removed. For detection of *NeuT* (*ErbB2*) phosphorylation, 400 μg of total tumor lysates were precipitated with a human anti-ErbB2-monoclonal antibody. An aliquot was resolved by SDS-PAGE and blotted onto a polyvinylidene difluoride membrane. The membrane was then incubated with a monoclonal antihuman-Ptyr antibody. Phosphorylated ErbB2 (*Ptyr ErbB2*) was then visualized with antimouse-IgG using enhanced chemiluminescence technology. For detection of total *NeuT* (*ErbB2*) protein, 30 μg of total tumor lysates were resolved by SDS-PAGE, blotted onto a polyvinylidene difluoride membrane, then incubated with a polyclonal rabbit antihuman-ErbB2 antibody. The *NeuT* antibody complex was then visualized with antirabbit-IgG using enhanced chemiluminescence technology.

inhibition of growth factor-dependent proliferation of cells that express/overexpress the EGFR (mouse epidermal keratinocyte and NCI-H596 cells) or overexpress ErbB2 (BT-474 and SK-BR-3 cells), compared with the relative insensitivity of the ras-transformed T24 cells, strongly suggest that AEE788 indeed effectively and selectively targets both receptors at the cellular level. Of note, AEE788 also inhibits EGFRvIII-mediated proliferation and phosphorylation in 32D/EGFRvIII cells and blocks phosphorylation of EGFRvIII in MCF-7/EGFRvIII cell systems. Hence, AEE788 has potential as an anticancer agent also in tumors driven by this mutant receptor. Although AEE788 is a weaker KDR inhibitor (IC_{50} 77 nM) as compared with its EGFR/ErbB2 activity, it efficiently blocked VEGF-stimulated and EGF-stimulated proliferation in human umbilical vein endothelial cells at comparable concentrations (IC_{50}s = 159 and 43 nM, respectively), suggesting that both signal transduction pathways are affected in this endothelial cell system.

To aid the *in vivo* profiling of AEE788, we used a combination of PKI166 and PTK787/ZK222584 as a control to address the question of whether AEE788 exerts similar antitumor efficacy compared with a drug combination (blocking ErbB and VEGF receptor activity), which had already proven to act additively or synergistically (44). In three models (NCI-H596 lung, DU145 prostate, and *NeuT*/ErbB2 GeMag), AEE788, at a daily oral dose of 30 mg/kg (total weekly dose of 150 mg/kg), was within statistical significance similarly active as compared with a daily dose of 100 mg/kg of each combination partner (total weekly dose of 1000 mg/kg). Interestingly, AEE788 elicited its most potent antitumor effect in the orthotopic ErbB2-driven *NeuT*/GeMag model. It is also noteworthy that an intermittent dose of 50 mg/kg of AEE788, given three times a week, still showed considerable antitumor activity, suggestive of long compound residency in tumor tissue. Indeed, the pharmacokinetic profile after a single oral dose of AEE788 was characterized by a rapid uptake into the circulation followed by a slow elimination phase. Furthermore, there was a substantially (20-fold) higher exposure of the compound in tumor tissue and other tissues (muscle and liver) as compared with plasma, such that after 24 h the tumor concentration was still ~50 μM. This high exposure and long residency of AEE788 in tumor fully translated into a long-lasting inhibition of EGFR and ErbB2 phosphorylation in tumor tissue. Specifically, treatment of mice with a daily, efficacious dose potently inhibited EGFR and ErbB2 phosphorylation in A431 and H-596 tumors for >72 h and inhibited ErbB2 phosphorylation in GeMag tumors for >24 h. These observations indicate that intermittent AEE788 treatment regimens could be applicable in the clinical setting.

On the basis of the above results, one cannot differentiate how much of the observed *in vivo* effects of AEE788 are due to its EGFR/ErbB2 inhibitory activity and how much due to direct antiangiogenic effects caused by VEGFR inhibition. This situation is complicated by the fact that antiangiogenic effects (*e.g.*, reduction of vascular permeability and reduction of diameter and volume of tumor

Table 6 *Inhibition of growth factor-induced vascularized tissue formation using the growth factor impregnated implant model in mice Results are from measurements of blood content of tissue that is surrounding the implant.*

	VEGF[a]-stimulated ED_{50} for inhibition of blood content[b]	bFGF-stimulated ED_{50} for inhibition of blood content[b]
AEE788	26;32	>100;>100
PTK787/ZK222584	29;42	30;42
PKI166	>100	nd

[a] VEGF, vascular endothelial growth factor; bFGF, basic fibroblast growth factor; nd, not determined.

[b] ED50 values are calculated from the dose-response curve from at least two independent experiments and were mg/kg p.o. per day.

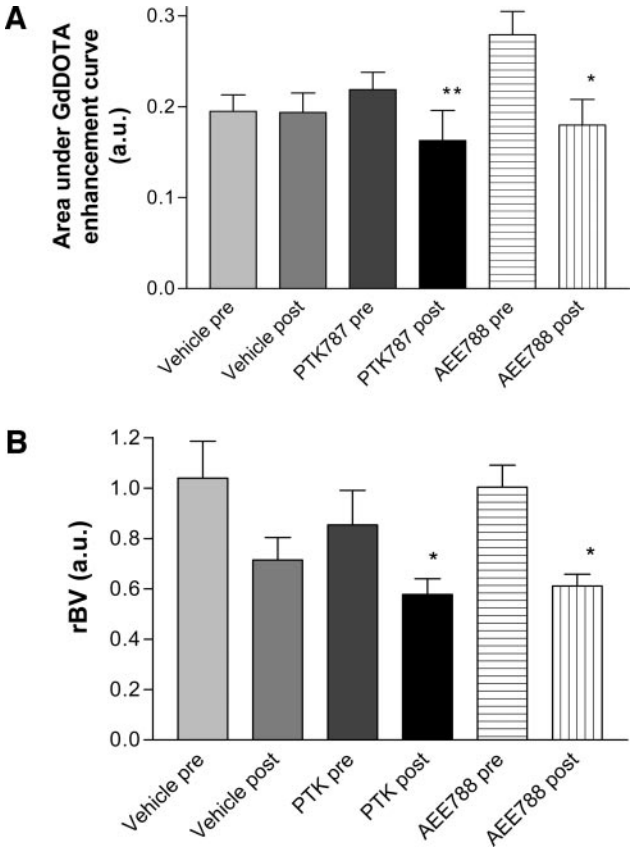

Fig. 8. Effects of AEE788 and PTK787/ZK222584 on the area under the enhancement curve and relative blood volume (*rBV*) of B16/BL6 cervical metastases measured by dynamic contrast enhanced-magnetic resonance imaging. C57/BL6 mice bearing established B16/BL6 tumors were treated daily for 3 days with 50 mg/kg AEE788, 100 mg/kg PTK787/ZK222584, or vehicle. Before (*pre*) and after (*post*) this treatment, dynamic contrast enhanced-magnetic resonance imaging analysis was performed on the cervical metastases. The area under the enhancement curve was determined from the area under the enhancement curve for GdDOTA (Dotarem; *A*) and the rBV from the plateau value (arbitrary units) of ENDODERM uptake (*B*). Shown are the means for paired animals ($n = 5$ vehicle; $n = 6$ test compounds), where $**P = 0.005$ and $*P \leq 0.02$ using 2-tailed paired *t* test; bars, ±SE.

blood vessels, and so forth) can be attributed to EGFR/ErbB2 inhibitors (*e.g.*, the recombinant antibody Herceptin; Ref. 40) and small molecule inhibitors Iressa (30) and PKI166 (42). Due to experimental difficulties, we have as yet been unable to show direct inhibition of KDR phosphorylation in tumor tissue derived from AEE788-treated mice. However, two *in vivo* findings do support the concept that AEE788 is also having direct antiangiogenic effects, as expressed by VEGFR kinase inhibition. In the VEGF- or bFGF-dependent growth factor implant model, used previously for the characterization of the potent VEGFR inhibitor PTK787/ZK222584 (7, 31), AEE788, but not the EGFR inhibitors PKI166 (Table 6), or Iressa (data not shown) dose-dependently inhibited VEGF-induced angiogenesis and showed similar ED_{50} values as observed for PTK787/ZK222584. Additionally, an antiangiogenic activity of AEE788 could clearly be demonstrated in the B16/BL6 metastatic melanoma mouse model using DCE-MRI technology. Strikingly, reductions of the area under the enhancement curve for GdDOTA and relative blood volume after oral treatment with an efficacious dose of AEE788 were significant and similar to those observed with PTK787/ZK222584. These are important findings, because the antiangiogenic effects of PTK787/ZK222584 as measured by DCE-MRI have not only been reported in preclinical models (47) but also in clinical trials (48). In these trials, conducted on colorectal patients exhibiting liver metastases, significant dose-dependent effects of PTK787/ZK222584 on tumor vascularization were observed to correlate with reductions in tumor burden and positive patient outcome. Indeed, these data contributed an integral part of the clinical proof of concept for this compound as a VEGFR inhibitor (48)

Altogether, the data presented here demonstrate that AEE788 not only acts through inhibition of the EGFR/ErbB2-mediated signal transduction pathway but also blocks VEGFR-mediated events. *In vivo* antitumor efficacy data correlate with the capacity of this compound to attain plasma and tumor levels that are: (*a*) in excess of *in vitro* IC_{50} values needed for the inhibition of activities related to EGFR/ErbB2 signal transduction (*e.g.*, inhibition of EGFR and ErbB2 phosphorylation/mediated proliferation); (*b*) sufficient to almost totally block EGFR and ErbB2 activity for long periods of time; and (*c*) sufficient to demonstrate antiangiogenic effects in a VEGF-driven implant model and as assessed by MRI technology. On the basis of this favorable preclinical profile, AEE788 has recently entered Phase I clinical trials in cancer patients.

ACKNOWLEDGMENTS

We thank Mike Becquet, Bruno Bohler, Stephane Ferretti, Gerard Goutte, Peter Haener, Claire Kowalik, Daniela Manfrina, Hans-Peter Mueller, Nicole Martin, Robert Reuter, Christian Schnell, Dario Sterker, Willi Theilkaes, Andreas Theuer, and Hong Yu for technical assistance.

REFERENCES

1. Woodburn JR. The epidermal growth factor receptor and its inhibition in cancer therapy. Pharmacol Ther 1999;82:241–50.
2. Matter A. Tumor angiogenesis as a therapeutic target. Drug Discovery Today 2001; 6:1005–24.
3. Voldborg BR, Damstrup L, Spang-Thomsen M, Poulsen HS. Epidermal growth factor receptor (EGFR) and EGFR mutations, function and possible role in clinical trials. Ann Onc 1997;8:1197–206.
4. Ciardiello F, Tortora G. A novel approach in the treatment of cancer: targeting the epidermal growth factor receptor. Clin Cancer Res 2002;7:2958–70.
5. Traxler P. Tyrosine kinases as targets in cancer therapy - successes and failures. Exp Opin Ther Targets 2003;7:215–34.
6. Mendelsohn J, Baselga J. The EGF receptor family as targets for cancer therapy. Oncogene 2000;19:6550–65.
7. Wood JM. Inhibition of vascular endothelial growth factor (VEGF) as a novel approach for cancer therapy. MEDICINA 2000;60(Suppl 2):41–7.
8. Bilodeau MT, Fraley ME, Hartman GD. Kinase insert domain-containing receptor kinase inhibitors as anti-angiogenic agents. Exp Opin Invest Drugs 2002;11:737–45.
9. Pegram M, Slamon D. Biological rationale for HER2/neu (c-erbB2) as a target for monocloncal antibody therapy. Semin Onocol 2000;5(Suppl. 9):13–9.
10. Moscatello DK, Holgado-Madruga M, Emlet DR, Montgomery RB, Wong AJ. Constitutive activation of phosphatidylinositol 3-kinase by a naturally occurring mutant epidermal growth factor receptor. J Biol Chem 1998;273:200–6.
11. Tang CK, Gong X-Q I, Moscatello DK, Wong AJ, Lippman ME. Epidermal growth factor receptor vIII enhances tumorgenicity in human breast cancer. Cancer Res 2000;60:3081–7.
12. Folkman J. Angiogenesis in cancer, vascular, rheumatoid and other disease. Nat Med (NY) 1995;1:27–31.
13. Parangi S, O'Reilly M, Christofori G, et al. Antiangiogenic therapy of transgenic mice impairs de novo tumor growth. Proc Natl Acad Sci USA 1996;93:2002–7.
14. Weinstat-Saslow D, Steeg PS. Angiogenesis and colonization in the tumor metastatic process: basic and applied advances. FASEB J 1994;8:401–7.
15. Folkman J. The role of angiogenesis in tumor growth. Semin Cancer Biol 1992;3: 65–71.
16. Breier G, Risau W. The role of vascular endothelial growth factor in blood vessel formation. Trends Cell Biol 1996;6:454–6.
17. Koelch W, Martiny-Baron G, Kieser A, Marme D. Regulation of the expression of the VEGF/VPS and its receptors: role in tumor angiogenesis. Breast Cancer Res Treat 1995;36:139–55.
18. Ferrara N. Vascular endothelial growth factor. Trends Cardiovasc Med 1993;3:244–50.
19. Neufeld G, Cohen T, Gengrinovitch S, Poltorak Z. Vascular endothelial growth factor (VEGF) and its receptors. FASEB J 1999;13:9–22.
20. Fong TA, Shawver LK, Sun L, et al. SU5416 is a potent and selective inhibitor of the vascular endothelial growth factor receptor (Flk-1/KDR) that inhibits tyrosine kinase catalysis, tumor vascularization, and growth of multiple tumor types. Cancer Res 1999;59:99–106.
21. Mendelsohn J. Epidermal growth factor receptor inhibition by a monoclonal antibody as anticancer therapy. Clin Cancer Res 1997;3:2703–7.
22. Mendelsohn J. Targeted therapy: the epidermal growth factor receptor. Prog Anti-Cancer Chemother 1999;2:106–11.

23. Zhang H, Richter M, Green M. Therapeutic monoclonal antibodies for the ErbB family of receptor tyrosine kinases. Cancer Biol Ther 2003;2(4 Suppl I):S122–6.
24. Furet P, Manley PW. Prospects for antiangiogenic therapies based upon VEGF inhibition. ACS Symposium Series 2001;796:282–98.
25. Mendel DB, Laird AD, Xin X, et al. In vivo antitumor activity of SU11248, a novel tyrosine kinase inhibitor targeting vascular endothelial growth factor and platelet-derived growth factor receptors: determination of a pharmacokinetic/pharmacodynamic relationship. Clin Cancer Res 2003;9:327–37.
26. Laird AD, Vajkoczy P, Shawver LK, et al. SU6668 is a potent antiangiogenic and antitumor agent that induces regression of established tumors. Cancer Res 2000;60: 4152–60.
27. Laird AD, Cherrington JM. Small molecule tyrosine kinase inhibitors: clinical development of anticancer agents. Exp Opin Invest Drugs 2003;12:51–6.
28. Fabbro D, Garcia-Echeverria CG. Targeting protein kinases in cancer therapy. Curr Opin Drug Disc Devel 2002;5:701–12.
29. Glade-Bender J, Kandel JJ, Yamashiro DlJ. VEGF blocking therapy in the treatment of cancer. Exp Opin Biol Ther 2003;3:263–76.
30. Wakeling AE, Guy SP, Woodburn JR, et al. ZD1839 (Iressa): An orally active inhibitor of epidermal growth factor signaling with potential for cancer therapy. Cancer Res 2002;62:5749–54.
31. Wood JM, Bold G, Buchdunger E, et al. PTK787/ZK 222584, a novel and potent inhibitor of vascular endothelial growth factor receptor tyrosine kinases, impairs vascular endothelial growth factor-induced responses and tumor growth after oral administration. Cancer Res 2000;60:2178–89.
32. Solorzano CC, Baker CH, Bruns CJ, et al. Inhibition of growth and metastasis of human pancreatic cancer growing in nude mice by PTK 787/ZK222584, an inhibitor of the vascular endothelial growth factor receptor tyrosine kinases. Cancer Biother Radiopharm 2001;16:359–70.
33. Drevs J, Hofmann I, Hugenschmidt H, et al. Effects of PTK787/ZK 222584, a specific inhibitor of vascular endothelial growth factor receptor tyrosine kinases, on primary tumor, metastasis, vessel density, and blood flow in a murine renal cell carcinoma model. Cancer Res 2000;60:4819–24.
34. Drevs J, Mross K, Medinger M, et al. Surrogate markers for the assessment of biological activity of the VEGF-receptor inhibitor PTK787/ZK222584 (PTK/ZK) in two clinical trials. Proc Am Soc Clin Oncol 2002;20:Abstract 337.
35. Hennequin LF, Thomas AP, Johnstone C, et al. Design and structure-activity relationship of a new class of potent VEGF receptor tyrosine kinase inhibitors. J Med Chem 1999;42:5369–89.
36. Wedge SR, Ogilvie DJ, Dukes M, et al. ZD6474 inhibits vascular endothelial growth factor signaling, angiogenesis, and tumor growth following oral administration. Cancer Res 2002;62:4645–55.
37. Hurwitz HI, Eckhardt SG, Holden SN, et al. A phase I study of ZD6474, an oral VEGF receptor tyrosine kinase inhibitor, in patients with solid tumors Proc AACR-NCI-EORTC. Clin Cancer Res 2001;7:5.
38. Goldman CK, Kim J, Wong WL, King V, Brock T, Gillespie GY. Epidermal growth factor stimulates vascular endothelial growth factor production by human malignant glioma cells: A model of glioblastoma multiforme pathophysiology. Mol Biol Cell 1993;4:121–33.
39. Maity A, Pore N, Lee J, Solomon D, O'Rourke DM. Epidermal growth factor receptor transcriptionally up-regulates vascular endothelial growth factor expression in human glioblastoma cells via a pathway involving phosphatidylinositol 3′-kinase and distinct from that induced by hypoxia. Cancer Res 2000;60:5879–88.
40. Izumi Y, Xu L, Di Tomaso E, Fukumura D, Jain RK. Tumor biology: herceptin acts as an anti-angiogenic cocktail. Nature 2002;416:279–80.
41. Petit AMV, Rak J, Hung MC, et al. Neutralizing antibodies against epidermal growth factor and ErbB-2/neu receptor tyrosine kinases down-regulate vascular endothelial growth factor production by tumor cells in vitro and in vivo: angiogenic implications for signal transduction therapy of solid tumors. Am J Pathol 1997;151:1523–30.
42. Bruns CJ, Solorzano CC, Harbison MT, et al. Blockade of the epidermal growth factor receptor signaling by a novel tyrosine kinase inhibitor leads to apoptosis of endothelial cells and therapy of human pancreatic carcinoma. Cancer Res 2000;60: 2926–35.
43. Shaheen RM, Ahmad SA, Liu W, et al. Inhibited growth of colon cancer carcinomatosis by antibodies to vascular endothelial and epidermal growth factor receptors. Br J Cancer 2001;85:584–9.
44. Brandt R, O'Reilly T, Wood J, Cozens R. Combined inhibition of EGF-receptor and VEGF-receptor kinases produces profound anti-tumor efficacy against experimental cancer. Proc Am Assoc Cancer Res 2002;43:Abstract 5352.
45. Brandt R, Wong AML, Hynes NE. Mammary glands reconstituted with Neu/ErbB2 transformed HC11 cells provide a novel orthotopic tumor model for testing anticancer agents. Oncogene 2001;20:5459–65.
46. Bold G, Altmann KH, Frei J, et al. New anilinophthalazines as potent and orally well absorbed inhibitors of the VEGF receptor tyrosine kinases useful as antagonists of tumor-driven angiogenesis. J Med Chem 2000; 43:2310–2323. Erratum in: J Med Chem 2000;43:3200.
47. Drevs J, Muller-Driver R, Wittig C, et al. PTK787/ZK 222584, a specific vascular endothelial growth factor-receptor tyrosine kinase inhibitor, affects the anatomy of the tumor vascular bed and the functional vascular properties as detected by dynamic enhanced magnetic resonance imaging. Cancer Res 2002;62:4015–22.
48. Morgan B, Thomas AL, Drevs J, et al. Dynamic contrast-enhanced magnetic resonance imaging as a biomarker for the pharmacological response of PTK787/ZK222584, an inhibitor of the vascular endothelial growth factor receptor tyrosine kinase, in patients with advanced colorectal cancer and liver metastasis: results from two Phase I studies. J Clin Oncol 2003;21:3955–64.

AEE788: A Dual Family Epidermal Growth Factor Receptor/ErbB2 and Vascular Endothelial Growth Factor Receptor Tyrosine Kinase Inhibitor with Antitumor and Antiangiogenic Activity

Peter Traxler, Peter R. Allegrini, Ralf Brandt, et al.

Cancer Res 2004;64:4931-4941.